Cyclic GMP–AMP signalling protects bacteria against viral infection

https://doi.org/10.1038/s41586-019-1605-5

Received: 25 June 2019

Accepted: 11 September 2019

Published online: 18 September 2019

Daniel Cohen[1,3], Sarah Melamed[1,3], Adi Millman[1], Gabriela Shulman[1], Yaara Oppenheimer-Shaanan[1], Assaf Kacen[2], Shany Doron[1], Gil Amitai[1]* & Rotem Sorek[1]*

The cyclic GMP–AMP synthase (cGAS)–STING pathway is a central component of the cell-autonomous innate immune system in animals[1,2]. The cGAS protein is a sensor of cytosolic viral DNA and, upon sensing DNA, it produces a cyclic GMP–AMP (cGAMP) signalling molecule that binds to the STING protein and activates the immune response[3–5]. The production of cGAMP has also been detected in bacteria[6], and has been shown, in *Vibrio cholerae*, to activate a phospholipase that degrades the inner bacterial membrane[7]. However, the biological role of cGAMP signalling in bacteria remains unknown. Here we show that cGAMP signalling is part of an antiphage defence system that is common in bacteria. This system is composed of a four-gene operon that encodes the bacterial cGAS and the associated phospholipase, as well as two enzymes with the eukaryotic-like domains E1, E2 and JAB. We show that this operon confers resistance against a wide variety of phages. Phage infection triggers the production of cGAMP, which—in turn—activates the phospholipase, leading to a loss of membrane integrity and to cell death before completion of phage reproduction. Diverged versions of this system appear in more than 10% of prokaryotic genomes, and we show that variants with effectors other than phospholipase also protect against phage infection. Our results suggest that the eukaryotic cGAS–STING antiviral pathway has ancient evolutionary roots that stem from microbial defences against phages.

Bacterial antiphage immune systems, such as CRISPR–Cas and restriction modification systems, tend to concentrate in 'defence islands' in bacterial genomes[8]; this property has facilitated the discovery of defence systems on the basis of their colocalization with known ones[9–11]. We noticed that homologues of the gene that encodes cGAS in *V. cholerae* (*dncV*; 'dinucleotide cyclase in *Vibrio*') frequently tend to appear near defence genes. Out of 637 homologues of this protein that we identified through a homology search in 38,167 microbial genomes, we found that 417 (65.5%) are located in the vicinity of known defence systems (Fig. 1a). It has previously been shown that such a high propensity of colocalization with defence genes is a strong predictor that the gene under inspection has a role in phage resistance[11]. These results therefore suggest that the gene that encodes the bacterial cGAS participates in defence against phages.

The bacterial cGAS and the effector phospholipase 'cGAMP-activated phospholipase in *Vibrio*' (CapV)[7] are encoded by adjacent genes in the *V. cholerae* genome and are probably expressed in a single operon[7]. The same operon also contains two additional genes, the presence of which next to the *capV-dncV* gene pair is conserved in the majority of cases (96%, 613 out of 637 homologues), suggesting that the putative functional defence system that involves bacterial cGAS comprises these four genes (Fig. 1a). As has previously been noted[7,12], the two additional genes encode proteins with domains that are known to be associated with the eukaryotic ubiquitin system: the E1 and E2 domains that are typical of ubiquitin transfer and ligation enzymes, and a JAB domain, which is similar to de-ubiquitinase enzymes that remove ubiquitin from target proteins (Fig. 1b).

To test whether the four-gene operon that contains cGAS is an antiphage defence system, we cloned the operon of *V. cholerae* serovar O1 biovar El Tor (hereafter, *V. cholerae* El Tor) or the homologous operon from *Escherichia coli* strain TW11681 into the laboratory strain *E. coli* MG1655, which naturally lacks this system. In both cases, the putative four-gene system was cloned together with its upstream and downstream intergenic regions to preserve promoters, terminators and other regulatory sequences. We then challenged *E. coli* MG1655 bacteria containing these four-gene systems with an array of phages that spans the three major families of tailed, double-stranded DNA phages (T2, T4, T6 and P1 from the *Myoviridae*; λ-vir, T5, SECphi18 and SECphi27 from the *Siphoviridae*; and T7 from the *Podoviridae*), as well as the single-stranded DNA phage SECphi17, of the *Microviridae* family.

Both the *V.-cholerae*-derived and the *E.-coli*-derived four-gene operons conferred defence against multiple phages. The system from *E. coli* provided 10–1,800-fold protection against 6 of the 10 phages that we tested, and the system from *V. cholerae* protected against 2 of the phages (Fig. 1c, Extended Data Fig. 1). None of the systems protected against the transformation of a multi-copy plasmid (Extended Data Fig. 2). The stronger protective effect that was observed for the *E.-coli*-derived system, as compared to that from *V. cholerae*, possibly stems from the higher compatibility of the former with the *E. coli* host and the coliphages

[1]Department of Molecular Genetics, Weizmann Institute of Science, Rehovot, Israel. [2]Department of Immunology, Weizmann Institute of Science, Rehovot, Israel. [3]These authors contributed equally: Daniel Cohen, Sarah Melamed. *e-mail: gil.amitai@weizmann.ac.il; rotem.sorek@weizmann.ac.il

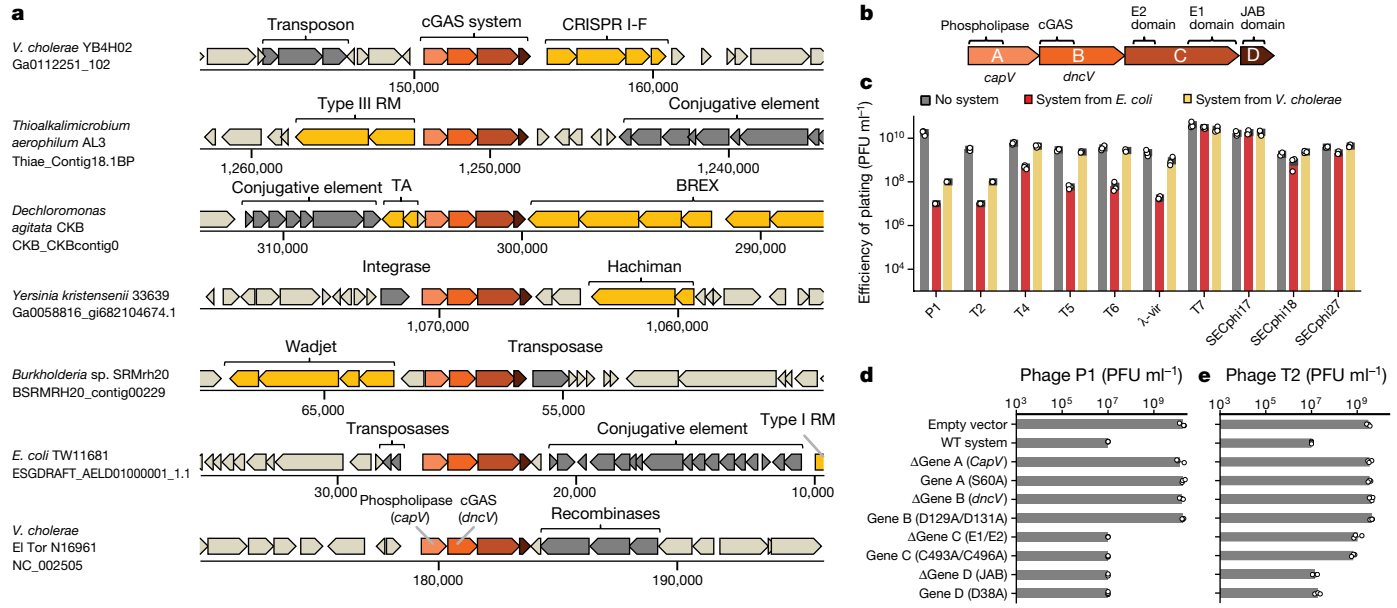

Fig. 1 | Systems containing bacterial cGAS protect against phage infection. **a**, Genes that encode bacterial cGAS are part of a conserved four-gene operon that is genomically associated with antiphage defence systems. Representative instances of the four-gene putative defence systems that contain cGAS, and their genomic environments, are presented. Genes that are known to be involved in defence are shown in yellow. Genes of mobile genetic elements are in dark grey. RM, restriction modification; TA, toxin–antitoxin. BREX, Hachiman and Wadjet are recently described defence systems[9,11]. **b**, Domain organization of the genes in the operon that contains cGAS. **c**, The four-gene operon from *V. cholerae* El Tor or *E. coli* TW11681 was cloned into *E. coli* MG1655 (Methods). The efficiency of plating is shown for ten phages infecting the control *E. coli* MG1655 strain (no system), the strain with the four-gene operon cloned from *E. coli* TW11681 (system from *E. coli*) and the strain with the four-gene operon cloned from *V. cholerae* El Tor (system from *V. cholerae*). Data represent plaque-forming units (PFU) per millilitre; bar graph represents average of three independent replicates, with individual data points overlaid. **d**, **e**, Efficiency of plating of phages infecting strains with the wild-type (WT) four-gene operon cloned from *E. coli* TW11681, deletion strains in that operon and strains with point mutations. Data represent plaque-forming units per millilitre; bar graph represents average of three independent replicates, with individual data points overlaid. Empty vector represents a control *E. coli* MG1655 strain that lacks the system and contains an empty vector instead. **d**, Infection with phage P1. **e**, Infection with phage T2.

that we used. We therefore proceeded with the *E.-coli*-derived system for further experiments.

To determine whether the ability to produce and sense cGAMP affects defence, we experimented with mutated forms of the system. Deletion of either the cGAS-encoding or the phospholipase-encoding genes resulted in a complete loss of protection against phage infection (Fig. 1d, e, Extended Data Fig. 3a–d). Moreover, point mutations in two essential aspartate residues in the cGAMP-producing active site of cGAS (D129A/D131A)[7,13] abolished defence, which suggests that cGAMP production is absolutely necessary for the phage-defensive properties of the system (Fig. 1d, e, Extended Data Fig. 3a–d). A S60A point mutation that inactivates the catalytic site of the CapV phospholipase also rendered the system completely inactive against all the phages that we tested, demonstrating that the cGAMP-controlled phospholipase activity of CapV is essential for defence (Fig. 1d, e, Extended Data Fig. 3a–d). These results indicate that, as in eukaryotes, the cGAS–cGAMP signalling pathway in bacteria participates in antiviral defence.

We next examined mutations in the two additional genes in the four-gene operon. Defence against the myophage P1 was not affected when the gene encoding the E1 and E2 domains or the gene encoding the JAB domain were deleted, which suggests that these two genes are not essential for protection against P1 (Fig. 1d). Accordingly, a construct that contained only the *capV-dncV* gene pair (that is, expressed only the phospholipase–cGAS pair) showed complete defence against P1 (Extended Data Fig. 4), demonstrating that the phospholipase–cGAS pair can work as a standalone defence system against some phages. However, deletion of the gene that encodes the E1 and E2 domains abolished defence against all of the other phages that were tested (T2, T4, T5, T6 and λ-vir). The presence of an intact gene that encodes the JAB-domain protein was necessary for protection against some phages (T4, T5 and T6), but not against others (P1, T2 and λ-vir). Point mutations that are predicted to inactivate the active site of the E1 domain (C493A/C496A) or to inactivate the active site of the peptidase in the JAB domain (D38A) recapitulated the results of deletions of the entire genes, suggesting that the predicted enzymatic activities of the E1–E2 and JAB proteins are necessary for their roles in phage defence (Fig. 1d, e, Extended Data Fig. 3a–d). Our mutational analyses suggest that the four-gene operon forms a bacterial system that relies on cGAMP signalling and phospholipase activity to defend against a broad range of phages, and that the activities of the two additional genes are necessary for defence against some—but not all—phages. We denote this system the cyclic-oligonucleotide-based antiphage signalling system (CBASS).

In animals, the sensing of viral infection is the trigger that activates the production of cGAMP[3]. We therefore sought to examine whether phage infection triggers the production of cGAMP in the bacterial system as well. To this end, we took advantage of the fact that the CapV phospholipase is activated by cGAMP, and used this protein as a reporter for the presence of cGAMP in infected cells. We first expressed and purified the CapV phospholipase from the *E. coli* CBASS system, and measured its activity using an in vitro phospholipase activity assay. As expected, chemically synthesized 3′3′-cGAMP induced CapV phospholipase activity in a concentration-dependent manner (Fig. 2a). Next, we exposed the purified CapV to cell lysates that were derived from cells containing the Δ*capV* CBASS, and which had been filtered to include small molecules only (Methods). The CapV phospholipase became markedly activated when exposed to cell lysates that were collected 40 min after infection with phage P1, which suggests that phage infection triggers cGAMP accumulation in cells that contain the CBASS (Fig. 2b). These results were corroborated by targeted mass spectrometry analysis, which detected cGAMP concentrations of 1.4–1.9 μM in lysates that were

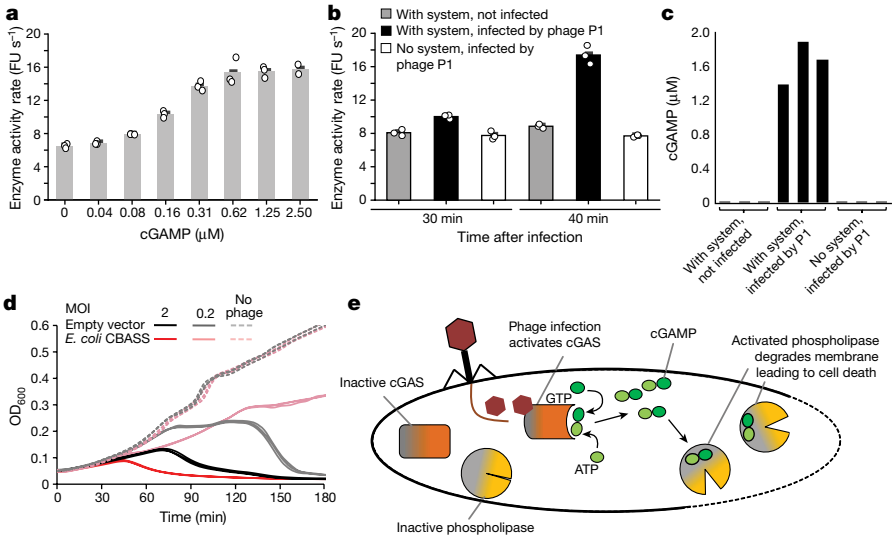

Fig. 2 | Phage infection triggers cGAMP accumulation and cell death. **a**, Purified CapV protein was incubated in vitro with synthetically produced 3′3′-cGAMP in the presence of resorufin butyrate, a phospholipase substrate that emits fluorescence when hydrolysed. The *x* axis shows the concentration of cGAMP added (μM); the *y* axis shows the enzyme activity rate, measured by the accumulation rate of fluorescence units (FU) per second (Methods). Bar graph represents average of three technical replicates, with individual data points overlaid (except for the 2.5 μM concentration, for which the data represent an average of two replicates). **b**, Purified CapV protein was incubated in vitro with filtered cell lysates derived from bacterial cultures infected by phage P1 at a multiplicity of infection (MOI) of 2. Lysates were extracted from cells containing the CBASS with the *capV* gene deleted ('with system') or from control cells that lack the CBASS and contain an empty vector instead ('no system'). Lysates were collected 30 min or 40 min after initial infection. Bar graph represents average of three technical replicates, with individual data points overlaid. **c**, Targeted mass spectrometry analysis was performed on the filtered cell lysates collected 40 min after initial infection by phage P1 at an MOI of 2. Lysates from uninfected samples were taken as control. The *y* axis represents the concentration of 3′3′-cGAMP in the cell lysate measured by mass spectrometry, as calculated on the basis of a calibration curve with synthetically produced 3′3′-cGAMP (Methods). Three independent replicates for each condition are shown, and each bar represents an individual replicate. **d**, Growth curves in liquid culture for bacteria that contain the CBASS and bacteria that lack the CBASS (empty vector), infected by phage P1 at 37 °C. Bacteria were infected at time 0 at an MOI of 0.2 or 2. OD_{600}, optical density at a wavelength of 600 nm. Three independent replicates are shown for each MOI, and each curve shows an individual replicate. **e**, Model for CBASS-based antiphage activity in bacteria.

collected 40 min after infection (Fig. 2c). CapV was not activated when exposed to lysates that were collected from uninfected cells, and only slightly activated by lysates that were collected from cells 30 min after infection. This implies that the phage component or cell state sensed by the CBASS appears in the cell relatively late in the phage-infection cycle (Fig. 2b).

It has previously been shown that, when stimulated by cGAMP, the CapV phospholipase degrades the membrane of *V. cholerae*, which leads to a loss of membrane integrity and to the arrest of cell growth or to death[7]. This, combined with our finding that the production of cGAMP is triggered by phage infection, led us to hypothesize that this defence system executes its defence via abortive infection. Abortive-infection defence systems exert their activity by causing the infected bacterial cell to 'commit suicide' before the phage replication cycle can be completed. This strategy eliminates infected cells from the bacterial population and protects the culture from a viral epidemic[14]. A phenotype such as this predicts that, with a high multiplicity of infection (MOI) (in which nearly all bacteria are infected in the first cycle), massive cell death will be observed in the culture, even for cells that contain the defence system.

To test this hypothesis, we infected bacteria growing in liquid cultures with phage P1 at varying MOIs and examined the culture dynamics. At an MOI of 0.2 (in which only around 20% of bacteria are initially infected by the phage) the culture of the wild-type cells collapsed owing to phage propagation, whereas the culture of the cells containing the CBASS was viable (Fig. 2d). Conversely, at an MOI of 2 (in which almost all bacteria are infected by the phage), the culture of wild-type cells and the culture of cells containing the CBASS both collapsed, which indicates cell lysis of the infected, CBASS-containing cells. Moreover, whereas at an MOI of 2 the wild-type culture started collapsing 70 min after initial infection (consistent with a time to lysis of 60–70 min after infection, as has previously been reported for phage P1[15]), the culture that contained the CBASS started collapsing as early as 45 min after infection—a period that is insufficient for the completion of the phage P1 replication cycle (Fig. 2d). These results were reproduced for other phages; when phages were applied at a high MOI, the cells that contained the CBASS showed lysis before the necessary time had elapsed for the completion of the phage replication cycle (Extended Data Fig. 5a). In the case of phage P1, the same phenotype was maintained for constructs that included only *capV-dncV* gene pair (that is, without the genes encoding the E1–E2 domains and JAB domain proteins), indicating that the latter two genes are not necessary for defence by abortive infection against phage P1 (Extended Data Fig. 5b).

These results were further corroborated by the staining of infected cells with propidium iodide, a fluorescent DNA-binding agent that is not membrane-permeable and cannot normally enter cells. Fluorescence-activated cell sorting (FACS) analysis showed that at 40 min after infection by phage P1 a substantial population of the cells that contain the CBASS became stained by propidium iodide, which indicates a loss of membrane integrity (Extended Data Fig. 6). This was associated with the loss of normal cell shape, as was observed via microscopy (Extended Data Fig. 7).

The above results suggest a model in which the cGAS–phospholipase defence system somehow senses a phage infection, and this sensing then triggers the production of cGAMP by the cGAS protein. The cGAMP molecule in turn activates the phospholipase, which degrades the bacterial membrane and causes cell death (Fig. 2e). This cell death before the completion of the phage replication cycle aborts the infection and prevents further propagation of the phage.

It has recently been shown that the bacterial cGAS gene (*dncV*) belongs to a large family of oligonucleotide cyclases, members of which are

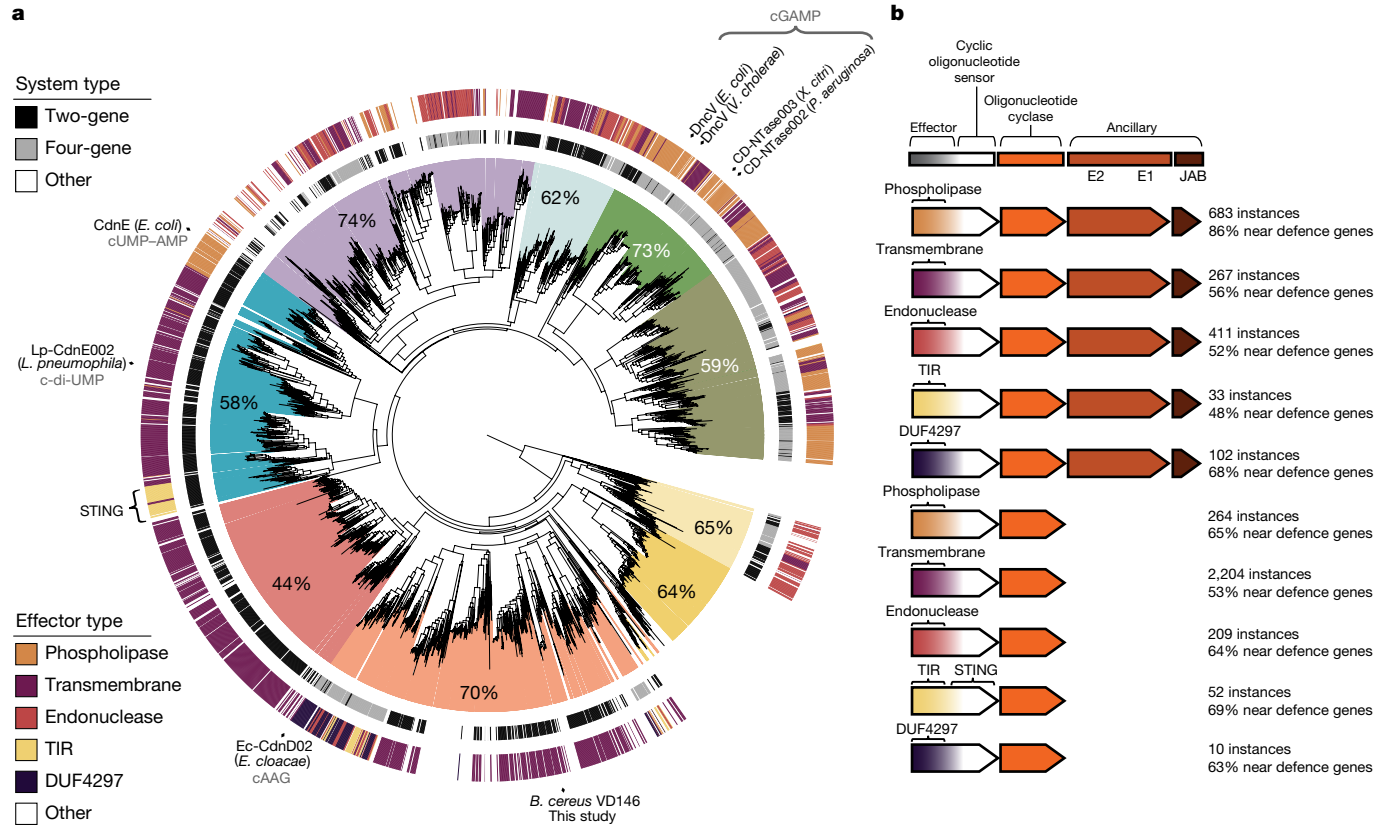

Fig. 3 | Widespread occurrence of CBASSs in prokaryotic genomes. **a**, Phylogenetic tree of proteins with predicted oligonucleotide cyclase domains that were identified by searching a set of 38,167 microbial genomes (Methods). Clades are coloured following a previous colour coding[16]. The percentage of genes that are located near known defence systems is indicated for each clade. The outermost ring indicates the type of effector gene that is associated with the oligonucleotide cyclase gene; bottom left, colour code for the effector types. The inner ring indicates the type of system: the two-gene system (comprising an oligonucleotide cyclase and an effector) or four-gene system (that also includes genes encoding the E1–E2 domains and JAB domain proteins). Top left, colour code for system type. Selected oligonucleotide cyclase genes that were biochemically characterized[16] are indicated; the cyclic oligonucleotide that each produces appears in grey font. cAAG, cyclic trinucleotide AMP–AMP–GMP. *E. cloacae*, *Enterobacter cloacae*; *L. pneumophila*, *Legionella pneumophila*; *P. aeruginosa*, *Pseudomonas aeruginosa*; *X. citri*, *Xanthomonas citri*. **b**, Common configurations of four-gene and two-gene CBASSs. The identified number of instances of each such system, and the percentage occurrence next to known defence systems, are indicated for each configuration.

found in about 10% of all sequenced bacterial genomes[16]. Other genes in this family synthesize a diverse set of cyclic oligonucleotide molecules, including cyclic UMP–AMP, cyclic di-UMP and even the cyclic trinucleotide AMP–AMP–GMP[16]. This family of genes has been divided into several clades on the basis of sequence similarity between its members[16]. We found that all major clades of this gene family have a high propensity to be genomically associated with other known defence genes in defence islands (Fig. 3a). Between 44% and 74% of the genes in each clade are located near known defence systems, which suggests that this entire family of oligonucleotide cyclases participates in phage defence (Fig. 3a).

When examining the genomic environment of the 6,232 genes that we identified as belonging to this family (Supplementary Table 1, Methods), we found that in 26% of the cases (1,612 instances) they appeared as part of a four-gene operon that resembled the CBASS of *V. cholerae* (including the genes encoding the E1–E2 domains and the JAB-domain proteins). In 683 (42%) of these operons the predicted effector gene had a phospholipase domain, but in the remaining cases the phospholipase domain in the effector gene was replaced by another domain (Fig. 3b). Common alternative effector domains included endonucleases (usually of the HNH type); a domain comprising predicted transmembrane helices; a domain of unknown function (DUF4297) that has previously been shown to participate in the Lamassu phage-resistance system[11]; and a Toll interleukin receptor (TIR) domain that was also previously shown to participate in antiphage defence[11] (Fig. 3b). These observations imply that in these variants of the CBASS, the alternative domains replace the phospholipase in exerting the cell-suicide effector activity. For example, the endonuclease may degrade cellular DNA and the transmembrane-domain effector may oligomerize to form membrane pores, as in the case of the RexA–RexB abortive infection system[17].

In addition, and consistent with previous reports[18], we found 2,745 cases in which the genes that belong to the family of oligonucleotide cyclases appeared in the context of a two-gene operon that lacked the genes encoding the E1–E2 domains and JAB-domain proteins. The second gene in the operon also frequently included phospholipase, endonuclease or transmembrane helix domains, which suggests that these operons represent a minimal CBASS that comprises only two genes (Fig. 3b). The most common predicted effector domain in these operons was a domain that included either two or four transmembrane helices; effector domains of this type are present in over 2,000 instances of the two-gene operons that we identified.

To test whether predicted two-gene CBASSs have a role in phage resistance, we examined a two-gene system from *Bacillus cereus* VD146 that contains a predicted effector gene with four transmembrane helices (Extended Data Fig. 8a). We engineered this system into the laboratory strain *Bacillus subtilis* BEST7003 and challenged the engineered strain with an array of 11 *Bacillus* phages, as previously described[11] (Methods). The system conferred strong defence against one of these phages (the myophage SBSphiC), verifying its ability to defend against phages

(Extended Data Fig. 8b). Deletion of the cGAS-like gene or of the effector gene rendered the system inactive (Extended Data Fig. 8b). Finally, infection assays of bacteria that contained the two-gene system in liquid culture showed culture collapse at a high MOI, consistent with an abortive infection system (Extended Data Fig. 8c).

We observed 52 instances of a two-gene CBASS in which the effector gene contained an N-terminal TIR domain, and also a C-terminal STING domain (Fig. 3b, Extended Data Fig. 9). Such a domain arrangement of STING fused to a TIR domain is also found in primitive eukaryotes, including the oyster *Crassostrea gigas* and the annelid worm *Capitella teleta*[1]. It is therefore possible that the CBASS with the TIR-STING effector gene represents the ancient evolutionary origin of the eukaryotic cGAS–STING system.

This study reveals the biological role of a large family of defence systems that is widespread in microbial genomes, but much remains unknown. The exact phage component sensed by the system is yet to be identified; it is unlikely that this component is cytoplasmic double-stranded DNA (as is the case in the animal cGAS–STING system), because bacteria do not have a nucleus and their cytoplasm therefore always contains double-stranded DNA. The role of the genes encoding the E1–E2 domains and JAB-domain proteins also remains unknown. These genes could be involved in the sensing of some phages, or in the mitigation of anti-cGAS activities that phages are likely to encode.

Accumulating evidence suggests that important components of the eukaryotic innate immune system have counterparts in bacterial immune systems. Argonaute—a central protein in the antiviral RNA interference machinery of plants, insects and animals[19]—has also been reported to have immunity roles in bacteria and archaea[20,21]. TIR domains, which are essential components of the pathogen-recognizing Toll-like receptors[22], are abundant in bacteria and have recently been shown to have a primary role in antiphage defence[11]. Foreign RNA is sensed in eukaryotic cells by the oligo-adenylate synthase (OAS) protein, leading to the activation of a non-specific RNase[23]; this process has recently been shown to have parallels in type III CRISPR–Cas immunity upon the sensing of phage RNA[24]. All of these processes, in addition to our finding that cGAS signalling in prokaryotes has an antiviral role similar to that in eukaryotes, are unlikely to have been the result of parallel evolution. Instead, these observations cumulatively point to a scenario in which these defence systems first evolved in prokaryotes as means of defence against phages, and the ancient eukaryote (which was probably formed by fusion of a bacterium and an archaeon[25]) inherited a primordial version of these systems from the prokaryotes that formed it. Under this hypothesis, these systems became the basis for the primitive immune system of the ancient eukaryote, and have evolved into the cell-autonomous immune system that we know today. If this hypothesis is correct, future studies may find homologues of additional components of the human immune system functioning as phage resistance systems in bacteria.

Online content

Any methods, additional references, Nature Research reporting summaries, source data, extended data, supplementary information, acknowledgements, peer review information; details of author contributions and competing interests; and statements of data and code availability are available at https://doi.org/10.1038/s41586-019-1605-5.

1. Kranzusch, P. J. et al. Ancient origin of cGAS-STING reveals mechanism of universal 2′,3′ cGAMP signaling. *Mol. Cell* **59**, 891–903 (2015).
2. Margolis, S. R., Wilson, S. C. & Vance, R. E. Evolutionary origins of cGAS-STING signaling. *Trends Immunol.* **38**, 733–743 (2017).
3. Sun, L., Wu, J., Du, F., Chen, X. & Chen, Z. J. Cyclic GMP-AMP synthase is a cytosolic DNA sensor that activates the type I interferon pathway. *Science* **339**, 786–791 (2013).
4. Ablasser, A. et al. cGAS produces a 2′-5′-linked cyclic dinucleotide second messenger that activates STING. *Nature* **498**, 380–384 (2013).
5. Ishikawa, H., Ma, Z. & Barber, G. N. STING regulates intracellular DNA-mediated, type I interferon-dependent innate immunity. *Nature* **461**, 788–792 (2009).
6. Davies, B. W., Bogard, R. W., Young, T. S. & Mekalanos, J. J. Coordinated regulation of accessory genetic elements produces cyclic di-nucleotides for *V. cholerae* virulence. *Cell* **149**, 358–370 (2012).
7. Severin, G. B. et al. Direct activation of a phospholipase by cyclic GMP-AMP in El Tor *Vibrio cholerae*. *Proc. Natl Acad. Sci. USA* **115**, E6048–E6055 (2018).
8. Makarova, K. S., Wolf, Y. I., Snir, S. & Koonin, E. V. Defense islands in bacterial and archaeal genomes and prediction of novel defense systems. *J. Bacteriol.* **193**, 6039–6056 (2011).
9. Goldfarb, T. et al. BREX is a novel phage resistance system widespread in microbial genomes. *EMBO J.* **34**, 169–183 (2015).
10. Ofir, G. et al. DISARM is a widespread bacterial defence system with broad anti-phage activities. *Nat. Microbiol.* **3**, 90–98 (2018).
11. Doron, S. et al. Systematic discovery of antiphage defense systems in the microbial pangenome. *Science* **359**, eaar4120 (2018).
12. Iyer, L. M., Burroughs, A. M. & Aravind, L. The prokaryotic antecedents of the ubiquitin-signaling system and the early evolution of ubiquitin-like β-grasp domains. *Genome Biol.* **7**, R60 (2006).
13. Kato, K., Ishii, R., Hirano, S., Ishitani, R. & Nureki, O. Structural basis for the catalytic mechanism of DncV, bacterial homolog of cyclic GMP-AMP synthase. *Structure* **23**, 843–850 (2015).
14. Molineux, I. J. Host–parasite interactions: recent developments in the genetics of abortive phage infections. *New Biol.* **3**, 230–236 (1991).
15. Walker, J. T. & Walker, D. H. Mutations in coliphage P1 affecting host cell lysis. *J. Virol.* **35**, 519–530 (1980).
16. Whiteley, A. T. et al. Bacterial cGAS-like enzymes synthesize diverse nucleotide signals. *Nature* **567**, 194–199 (2019).
17. Snyder, L. Phage-exclusion enzymes: a bonanza of biochemical and cell biology reagents? *Mol. Microbiol.* **15**, 415–420 (1995).
18. Burroughs, A. M., Zhang, D., Schäffer, D. E., Iyer, L. M. & Aravind, L. Comparative genomic analyses reveal a vast, novel network of nucleotide-centric systems in biological conflicts, immunity and signaling. *Nucleic Acids Res.* **43**, 10633–10654 (2015).
19. Joshua-Tor, L. & Hannon, G. J. Ancestral roles of small RNAs: an Ago-centric perspective. *Cold Spring Harb. Perspect. Biol.* **3**, a003772 (2011).
20. Swarts, D. C. et al. DNA-guided DNA interference by a prokaryotic argonaute. *Nature* **507**, 258–261 (2014).
21. Olovnikov, I., Chan, K., Sachidanandam, R., Newman, D. K. & Aravin, A. A. Bacterial argonaute samples the transcriptome to identify foreign DNA. *Mol. Cell* **51**, 594–605 (2013).
22. Akira, S. & Takeda, K. Toll-like receptor signalling. *Nat. Rev. Immunol.* **4**, 499–511 (2004).
23. Zhou, A. et al. Interferon action and apoptosis are defective in mice devoid of 2′,5′-oligoadenylate-dependent RNase L. *EMBO J.* **16**, 6355–6363 (1997).
24. Kazlauskiene, M., Kostiuk, G., Venclovas, Č., Tamulaitis, G. & Siksnys, V. A cyclic oligonucleotide signaling pathway in type III CRISPR-Cas systems. *Science* **357**, 605–609 (2017).
25. Margulis, L. Archaeal–eubacterial mergers in the origin of Eukarya: phylogenetic classification of life. *Proc. Natl Acad. Sci. USA* **93**, 1071–1076 (1996).

Methods

No statistical methods were used to predetermine sample size. The experiments were not randomized and investigators were not blinded to allocation during experiments and outcome assessment.

Genomic identification and analysis of DncV homologues

The protein sequence of DncV (NCBI accession NP_229836) was searched against the protein sequences of all genes in 38,167 bacterial and archaeal genomes downloaded from the Integrated Microbial Genomes (IMG) database[26] in October 2017, using the 'search' option in the MMseqs2 package[27] (release 6-f5a1c) with default parameters. Hits with an *e* value less than 1×10^{-20} were taken as homologues. The fraction of homologues found in the vicinity of known defence systems was calculated as previously described[11], using a positive set of defence gene families that was updated to include a recently discovered set of defence genes[11].

Genomic analysis of oligonucleotide cyclase genes

For the analysis in Fig. 3, the proteins from the database of 38,167 bacterial and archaeal genomes were first clustered using the 'cluster' option of MMseqs2[27] (release 2-1c7a89), with default parameters. Clusters were further aggregated into larger clusters using four additional cycles of clustering, in which—in each cycle—a representative sequence was taken from each cluster using the 'createsubdb' option of MMseqs2 and representative sequences were clustered using the 'cluster' option with the '–add-self-matches' parameter. For the first additional clustering cycle, the 'cluster' option was run with default parameters; for the additional cycles 2–4, clustering was run with sensitivity parameter '-s 7.5', and for the additional cycle 4, the '–cluster-mode 1' parameter was also added.

The sequences of each cluster were aligned using Clustal Omega[28]. Each multiple sequence alignment was scanned with HHpred[29] using 60% gap rule (-M 60) against the PDB_mmCIF70[30] and pfam31[31] databases. Clusters with HHpred hits to one of the cGAS entries (Protein Data Bank (PDB) codes: 4LEV, 4MKP, 4O67, 5VDR, 5V8H, 4LEW, 5VDP, 4KM5, 4O68, 4O69, 5V8J, 5V8N, 5V8O, 5VDO, 5VDQ, 5VDS, 5VDT, 5VDU, 5VDV, 5VDW, 4XJ5, 4XJ1, 4XJ6, 4XJ3 and 4XJ4, and pfam PF03281) with >90% probability in the top 30 hits were taken for manual analysis. Clusters containing genes that were suspected to belong to toxin–antitoxin gene pairs were discarded. Overall, this procedure identified 30 clusters containing 6,232 predicted oligonucleotide cyclase genes from 5,150 genomes.

The genomic environments spanning 10 genes upstream and downstream of each of the 6,232 predicted oligonucleotide cyclase genes were searched to identify conserved gene cassettes and known defence genes around the oligonucleotide cyclase genes, as previously described[11]. Predicted systems were manually reviewed and unrelated genes (for example, mobilome genes and genes of other defence systems) were omitted.

To generate the phylogenetic tree in Fig. 3a, the 'clusthash' option of MMseqs2 (release 6-f5a1c) was first used to remove protein redundancies (using the '–min-seq-id 0.9' parameter). Sequences shorter than 200 amino acids were also removed. To further remove outlier sequences, an all-versus-all search was conducted using the 'search' option in MMseqs2, and proteins with less than 20 hits were manually examined. Overall, 17 outlier proteins were removed this way. The human cGAS protein (UniProt Q8N884) was added, as well as the human oligoadenylate synthase genes (UniProt P00973, P29728 and Q9Y6K5); these were used as an outgroup. Sequences were aligned using MAFFT[28] with gap open penalty of '–op 2'. The FastTree software[32] was used to generate a tree from the multiple sequence alignment using default parameters. The iTOL[33] software was used for tree visualization.

Cloning of the CBASS into *E. coli* MG1655

The following full-length constructs containing the CBASS were designed: the four-gene CBASS from *V. cholerae* El Tor N16961 (GenBank accession NC_002505) was identified as locus tags VC0178–VC0181, and the operon was taken together with its upstream and downstream intergenic regions, spanning the nucleotide range 178,424–183,957 in GenBank accession NC_002505. The four-gene system from *E. coli* TW11681 (GenBank accession AELD00000000) was identified as locus tags ESGDRAFT_00026–ESGDRAFT_00029 and the operon, together with its upstream and downstream intergenic regions, spanned the nucleotide range 21,738–27,072 in GenBank accession AELD00000000. These two constructs were commercially synthesized and cloned by Genscript directly into the plasmid pSG1-rfp[10,11] between the AscI and NotI sites of the multiple cloning site.

For strains with gene deletions and point mutations, plasmids containing systems with these deletions or mutations were also commercially synthesized and cloned into the plasmid pSG1-rfp by Genscript, except for one construct in which the genes for both the E1–E2 domains and JAB domain were deleted (used for Extended Data Figs. 4, 5b). To build this construct, the pSG1-rfp backbone was amplified with primers P1-Fw + P1-Rv using KAPA HiFi HotStart ReadyMix (Kapa Biosystems KK2601) (Supplementary Table 2). Primers P2-Fw + P2-Rv were used to lift the gene pair *capV* and *dncV* with their native promoter from the plasmid that contained the full system derived from *E. coli* TW11681 (Supplementary Table 2). After gel purification of the PCR products with Zymoclean Gel DNA Recovery Kit (cat. no. D4001), the two fragments were assembled using NEBuilder HiFI DNA Assembly cloning kit (NEB E5520S) to produce the construct that lacks both gene C (encoding the protein with the E1 and E2 domains) and gene D (encoding the JAB-domain protein).

The plasmids were transformed into *E. coli* MG1655 cells by electroporation, and the resulting transformants of the wild-type and mutated systems were verified by whole genome sequencing as previously described[10] to verify system integrity and a lack of mutations. A negative control was constructed as a transformant containing an empty pSG1 plasmid.

Cloning of the CBASS from *B. cereus* into *B. subtilis* BEST7003

The two-gene CBASS from *B. cereus* VD146 (GenBank accession KB976672) was identified as locus tags IK1_05630–IK1_05631, and the operon was taken together with its upstream and downstream intergenic regions, spanning the nucleotide range 60,974–63,493 in GenBank accession KB976672. The construct, as well as two additional constructs in which one of the two genes was deleted, were commercially synthesized and cloned by Genscript directly into the plasmid pSG1-rfp[10,11] between the AscI and NotI sites of the multiple cloning site. The plasmid was transformed into *B. subtilis* and integrated into the *amyE* locus as previously described[11]. A negative control was constructed as a transformant containing an empty pSG1 plasmid integrated in the *amyE* locus. The resulting transformants of the wild-type and mutated systems were verified by whole genome sequencing as previously described[10].

Phage cultivation

E. coli phages (P1, T4, T5, T7 and λ-vir) were provided by U. Qimron. Phages SECphi17, SECphi18 and SECphi27 were isolated in our laboratory[11]. T2 and T6 were ordered from the Deutsche Sammlung von Mikroorganismen und Zellkulturen (DSMZ) (DSM 16352 and DSM 4622, respectively). The following *B. subtilis* phages were obtained from the *Bacillus* Genetic Stock Center (BGSC): SPO1 (BGSCID 1P4), φ3T (BGSCID 1L1), SPβ (BGSCID 1L5), SPR (BGSCID 1L56), φ105 (BGSCID 1L11), ρ14 (BGSCID 1L15), SPP1 (BGSCID 1P7), SP82G (BGSCID 1P5). Phage φ29 was obtained from the DSMZ (DSM 5546). Phages SBSphiJ and SBSphiC were isolated in our laboratory[11]. Phages were propagated on *E. coli* MG1655 or *B. subtilis* BEST7003 in liquid culture, and their titre was determined using the small drop plaque assay method, as previously described[11].

Plaque assays

Bacteria were mixed with MMB agar (LB + 0.1 mM $MnCl_2$ + 5 mM $MgCl_2$ + 0.5% agar), and tenfold serial dilutions of the phage lysate in MMB were dropped on top of them. After the drops were dry, plates were

incubated overnight at 37 °C for *E. coli* phage and at room temperature for *B. subtilis* phages. Plaques were counted to calculate the efficiency of plating in plaque-forming units per millilitre. For phages showing a fuzzy killing zone in which single plaques could not be counted, the lowest phage concentration in which a killing zone was observed was counted as ten plaques. Fold defence was calculated as the efficiency of plating on control bacteria divided by the efficiency of plating value obtained on bacteria containing the CBASS.

Phage-infection dynamics in liquid medium

Overnight cultures were diluted 1:100 in MMB medium and incubated at 37 °C while shaking at 250 r.p.m. until early log phase (OD_{600} = 0.3). One hundred and eighty microlitres of the diluted culture were transferred into wells in a 96-well plate containing 20 µl of phage lysate for a final MOI of 2, 0.2 or 0.02 as applicable. Infections were performed in triplicate and OD_{600} was followed using a TECAN Infinite 200 plate reader with measurement every 5 min.

Transformation efficiency assay

To prepare electro-competent cells, *E. coli* MG1655 cells (with or without the CBASS) were diluted 1:100 in 100 ml LB medium supplemented with ampicillin, 100 µg/ml. At OD_{600} = 0.6, the cells were transferred to ice for 15 min and then centrifuged for 15 min at 4,000 r.p.m. The supernatant was discarded and the pellet was resuspended in ultrapure ice-cold water. This step was repeated twice and the supernatant was removed. The resultant pellet was resuspended in 10% glycerol, centrifuged for another 10 min and the supernatant was discarded. The final pellet was mixed in 500 µl of 10% glycerol and aliquots of 50 µl were flash-frozen in liquid nitrogen and transferred immediately to −80 °C.

One hundred nanograms of pRSFDuet-1 was added to 50 µl electro-competent cells and the mixture was transferred to a Bio-Rad Gene Pulser Curvette (0.2 cm, cat. no. 165-2086). The cells were electroporated with a Bio-Rad Micropulser using the 'Ec1' setting and then immediately transferred to 1 ml LB medium to recover at 37 °C for 1 h. After incubation cells were diluted 1:100, and 100 µl were plated on LB plates containing ampicillin (100 µg/ml) and kanamycin (50 µg/ml), and incubated at 37 °C overnight. Transformation efficiency was calculated by dividing the number of transformants that grew on LB plates containing ampicillin and kanamycin by the live count grown on LB ampicillin (100 µg/ml) only.

Cloning, expression and purification of CapV from *E. coli* TW11681

The CapV protein from *E. coli* TW11681 was PCR-amplified (primers P3-Fw + P3-Rv, and P4-Fw + P4-Rv), fused with a C-terminal His tag (linker plus His tag sequence: $SerGly_4His_6$) and cloned into pET28b. The plasmid was transformed into BL21(DE3)pLys cells and grown at 37 °C, 250 r.p.m., until induction (1 mM IPTG) at an OD_{600} of 0.6. After induction, bacterial cell culture growth was continued for an additional 14 h at a temperature of 18 °C. Cells were then centrifuged for 10 min (3,900*g*, 4 °C) and pellets kept at −20 °C. Pellets were thawed on ice and resuspended with an ice-cold buffer containing 50 mM phosphate buffer (pH 7.4), 300 mM NaCl, 10% glycerol (v/v). The buffer was supplemented with 10 µg/ml lysozyme, and 1 µl benzonase-nuclease (5KU Merck). The suspension was then mixed with Lysing matrix B (MP) beads and cells were disrupted mechanically using a FastPrep-24 (MP) bead-beater device (2 cycles of 40 s, 6 m s^{-1}). Cell lysate was centrifuged at 12,000*g* for 10 min at 4 °C and the supernatant was then mixed with Ni-NTA magnetic agarose beads (Qiagen) for 2 h (4 °C). CapV–6×His proteins bound to Ni-NTA beads were washed 3 times with a 50 mM phosphate buffer (pH 7.4), 300 mM NaCl, 10% glycerol (v/v), 20 mM imidazole and then eluted with the 50 mM phosphate buffer (pH 7.4), 300 mM NaCl, 10% glycerol (v/v), 250 mM imidazole. The eluent was loaded onto an Amicon Ultra-0.5 centrifugal filter unit 10-kDa filter (Merck) to exchange the elution buffer with the reaction buffer (50 mM phosphate buffer (pH 7.4), 300 mM NaCl, 10% glycerol (v/v)). Buffer exchange was done by centrifuging the centrifugal filter unit at 14,000*g* for 10 min at 4 °C 4 times with the reaction buffer. Eluted protein purification was assessed by running the sample on an SDS–PAGE gel and quantity was measured by using a Qubit Protein Assay Kit (Thermo Fisher Scientific).

Fluorogenic biochemical assay for CapV activity

The esterase activity of the 6×His-tagged CapV was probed with the fluorogenic substrate resorufin butyrate. The 6×His-tagged CapV was diluted in 50 mM sodium phosphate (pH 7.4), 300 mM NaCl, 10% (v/v) glycerol to a final concentration of 1.77 µM. To measure the linear range of CapV activation, purified 6×His-tagged CapV was incubated for 5 min with increasing concentrations of 3′3′-cGAMP (Merck), ranging from 0.04 to 2.5 µM of 3′3′-cGAMP. In parallel, 6×His-tagged CapV was incubated for 5 min with cell lysates derived from *E. coli* cells infected with phage P1 or uninfected. Subsequently, the enzyme–cGAMP or enzyme–lysate solution was added to DMSO-solubilized resorufin butyrate (stock of 20 mM mixed with 50 mM sodium phosphate (pH 7.4), 300 mM NaCl, 10% (v/v) glycerol reaching a final concentration of 64 µM (final assay DMSO concentration was 0.32%)) to a final assay volume of 50 µl, and fluorescence was measured in a 96-well plate (Corning 96-well half area black non-treated plate with a flat bottom). Plates were read once every 30 s for 10 min at 37 °C using an Infinite-200 (Tecan) with excitation and emission wavelengths of 550 and 591 nm, respectively. The enzymatic reaction velocity was measured as previously described[34]. For this, a regression fit was calculated for the output values of each reaction over time, and the slope of this linear regression fit was used for determining the initial reaction velocity (FU s^{-1}).

Cell lysate preparation

E. coli MG1655 cells containing the *E. coli* TW11681-derived CBASS in which the *capV* gene was deleted were used for preparation of cell lysates. Cells containing an empty vector (pSG1) were used as control. Cells were grown in 100 ml MMB medium (flask size 250 ml) at 37 °C (250 r.p.m.) until reaching an OD_{600} of 0.3. Cells were then infected with 5 ml of phage P1 (titre of 10^{10} infective particles per millilitre, estimated MOI of 2). After 30 or 40 min from the initial infection, samples were collected and centrifuged at 3,900*g* for 5 min at 4 °C. Following centrifugation, pellets were kept on ice until resuspended in 600 µl buffer containing 50 mM sodium phosphate (pH 7.4), 300 mM NaCl and 10% (v/v) glycerol. The resuspended pellet was supplemented with 1 µl hen-lysozyme (Merck) (final hen-lysozyme concentration of 16 µg/ml). The resuspended cells were then mixed with Lysing matrix B (MP) beads and cells were disrupted mechanically using a FastPrep-24 (MP) bead-beater device (2 cycles of 40 s, 6 m s^{-1}, at 4 °C). Cell lysate was then centrifuged at 12,000*g* for 10 min at 4 °C and the supernatant was loaded onto a 3-kDa filter Amicon Ultra-0.5 centrifugal filter unit (Merck) and centrifuged at 14,000*g* for 30 min at 4 °C. The flow-through—containing substances smaller than 3 kDa—was used as the lysate sample for evaluating cGAMP production within the cells (Fig. 2).

Quantification of 3′3′-cGAMP by high-performance liquid chromatography and mass spectrometry (HPLC–MS)

Cell lysates were prepared as described in 'Cell lysate preparation'. Lysates collected at 40 min after infection were analysed by MS-Omics using ultra-performance liquid chromatography (UPLC) (Vanquish, Thermo Fisher Scientific) coupled with a high-resolution quadrupole-orbitrap mass spectrometer (Q Exactive HF Hybrid Quadrupole-Orbitrap, Thermo Fisher Scientific). An electrospray ionization interface was used as an ionization source. Analysis was performed in positive ionization mode. A calibration series of 3′3′-cGAMP (SML1232, Sigma-Aldrich) ranging 0.001 to 50 µM was prepared and a linear regression from 0.001 to 5 µM was used for cGAMP quantification.

FACS analysis of infected cells

Overnight cultures of *E. coli* MG1655 cells containing the *E. coli* TW11681-derived CBASS, and *E. coli* MG1655 cells containing an empty vector (pSG1), were diluted 1:100 in 0.5 ml MMB and grown at 37 °C and 500 rpm to an OD_{600} of 0.3. Cells were then infected with phage P1 (titre of 10^{10} infective particles per millilitre, estimated MOI of 2). At 40 min after infection, 40 µl of each culture were diluted into 2 ml of filtered PBS containing 1 µl of propidium iodide (Invitrogen LIVE/DEAD BacLight Bacterial Viability Kit (L7007)). The diluted bacteria were incubated in the dark in room temperature for five minutes and were then analysed by a BIORAD ZE5 Cell Analyzer. A 5-s agitation was performed and then 25,000 ungated events were recorded for both the CBASS-containing and CBASS-lacking cultures at 0.2 µl s^{-1}. Forward scatter and propidium iodide fluorescence were measured using the height (*H*) parameter. FlowJo v.10 was used to analyse and visualize the data.

Microscopy of infected cells

E. coli MG1655 cells that contain the *E. coli* TW11681-derived CBASS or the same CBASS with a point mutation of the phospholipase catalytic site (S60A) were grown in MMB medium at 37 °C. When growth reached an OD_{600} of 0.3, bacteria were infected with P1 phage (MOI of about 2). Five hundred microlitres of the infected samples were centrifuged at 10,000*g* for 2 min at 25 °C and resuspended in 5 µl of 1× phosphate-buffered saline (PBS), supplemented with 1 µg/ml membrane stain FM4-64 (Thermo Fisher Scientific T-13320) and 2 µg/ml DNA stain 4,6-diamidino-2-phenylindole (DAPI) (Sigma-Aldrich D9542-5MG). Cells were visualized and photographed using an Axioplan2 microscope (ZEISS) equipped with ORCA Flash 4.0 camera (HAMAMATSU). System control and image processing were carried out using Zen software version 2.0 (Zeiss).

Reporting summary

Further information on research design is available in the Nature Research Reporting Summary linked to this paper.

Data availability

Data that support the findings of this study are available within the article and its Extended Data and Supplementary Tables. GenBank accessions, locus tags and nucleotide ranges of the CBASSs appear in the Methods. IMG gene and genome ID number, contig ID and system and effector classification appear in Supplementary Table 1. Primer sequences for the CBASSs are available in Supplementary Table 2. Any other relevant data are available from the corresponding authors upon reasonable request.

26. Chen, I. A. et al. IMG/M v.5.0: an integrated data management and comparative analysis system for microbial genomes and microbiomes. *Nucleic Acids Res*. **47**, D666–D677 (2019).
27. Steinegger, M. & Söding, J. MMseqs2 enables sensitive protein sequence searching for the analysis of massive data sets. *Nat. Biotechnol*. **35**, 1026–1028 (2017).
28. Madeira, F. et al. The EMBL-EBI search and sequence analysis tools APIs in 2019. *Nucleic Acids Res*. **47**, W636–W641 (2019).
29. Zimmermann, L. et al. A completely reimplemented MPI bioinformatics toolkit with a new HHpred server at its core. *J. Mol. Biol*. **430**, 2237–2243 (2018).
30. Berman, H., Henrick, K. & Nakamura, H. Announcing the worldwide Protein Data Bank. *Nat. Struct. Biol*. **10**, 980 (2003).
31. El-Gebali, S. et al. The Pfam protein families database in 2019. *Nucleic Acids Res*. **47**, D427–D432 (2019).
32. Price, M. N., Dehal, P. S. & Arkin, A. P. FastTree: computing large minimum evolution trees with profiles instead of a distance matrix. *Mol. Biol. Evol*. **26**, 1641–1650 (2009).
33. Letunic, I. & Bork, P. Interactive tree of life (iTOL) v3: an online tool for the display and annotation of phylogenetic and other trees. *Nucleic Acids Res*. **44**, W242–W245 (2016).
34. Lam, V. et al. Resorufin butyrate as a soluble and monomeric high-throughput substrate for a triglyceride lipase. *J. Biomol. Screen*. **17**, 245–251 (2012).
35. Kelley, L. A., Mezulis, S., Yates, C. M., Wass, M. N. & Sternberg, M. J. E. The Phyre2 web portal for protein modeling, prediction and analysis. *Nat. Protocols* **10**, 845–858 (2015).

Acknowledgements We thank A. Leavitt and S. Sharir for assistance in DNA extraction, library preparation and sequencing, A. Bernheim for assistance in data visualization, and members of the Sorek laboratory for fruitful discussions. This study was supported in part by the Israel Science Foundation (personal grant 1360/16), the European Research Council (grant ERC-CoG 681203), the Ernest and Bonnie Beutler Research Program of Excellence in Genomic Medicine, and the Knell Family Center for Microbiology. A.M. was supported by a fellowship from the Ariane de Rothschild Women Doctoral Program.

Author contributions D.C., S.M. and G.A. led the study and performed all experiments unless otherwise indicated. A.M. performed the computational analyses that appear in Figs. 1 and 3. Y.O.-S. performed the microscopy analysis that appears in Extended Data Fig. 7. G.S. assisted with the plaque assays that appear in Fig. 1 and Extended Data Figs. 1 and 3. A.K. and S.D. performed the computational analyses that led to Extended Data Fig. 8. R.S. supervised the study and wrote the paper together with the team.

Competing interests R.S. is a scientific cofounder and consultant of BiomX Ltd, Pantheon Ltd and Ecophage Ltd.

Additional information
Supplementary information is available for this paper at https://doi.org/10.1038/s41586-019-1605-5.
Correspondence and requests for materials should be addressed to G.A. or R.S.
Peer review information *Nature* thanks Zhijian 'James' Chen, Karen Maxwell and the other, anonymous, reviewer(s) for their contribution to the peer review of this work.
Reprints and permissions information is available at http://www.nature.com/reprints.

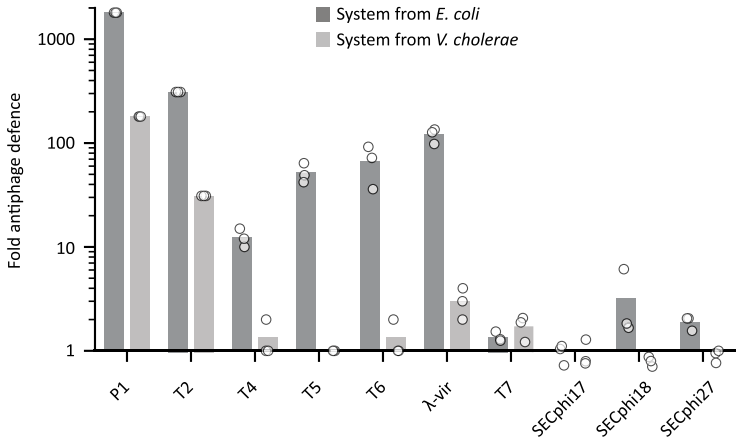

Extended Data Fig. 1 | Fold antiphage defence conferred by four-gene defence systems against various phages. The four-gene operon from either *V. cholerae* El Tor or *E. coli* TW11681 was cloned into *E. coli* MG1655 (Methods). Fold antiphage defence, as measured by plaque assays, is shown. The fold defence was calculated as the ratio between the efficiency of plating of the phage on the operon-lacking control strain and the efficiency of plating on the operon-containing strain (Fig. 2b, Methods). Bar graph represents average of three independent replicates, with individual data points overlaid. Points that fall below the *x* axis (for SECphi17, SECphi18 and SECphi27) denote values lower than 1.

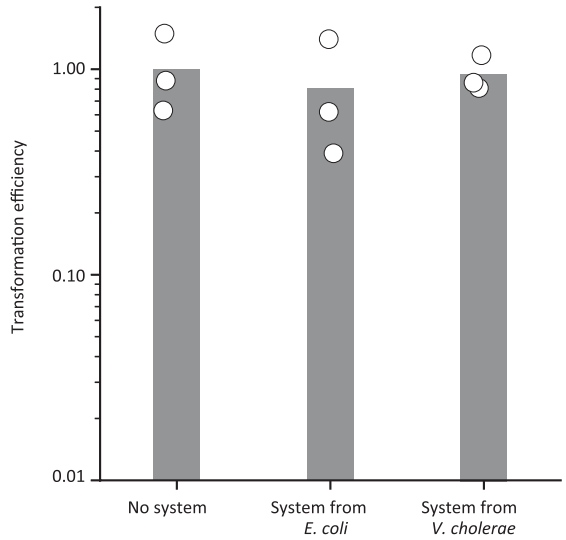

Extended Data Fig. 2 | Transformation efficiency assays. Transformation efficiency of plasmid pRSFDuet-1 into strains that contain the four-gene operon derived from *E. coli* TW11681 or from *V. cholerae* El Tor, presented as a fraction of the transformation efficiency to *E. coli* MG1655 carrying an empty vector instead of the four-gene operon. Bar graph represents average of three independent replicates, with individual data points overlaid.

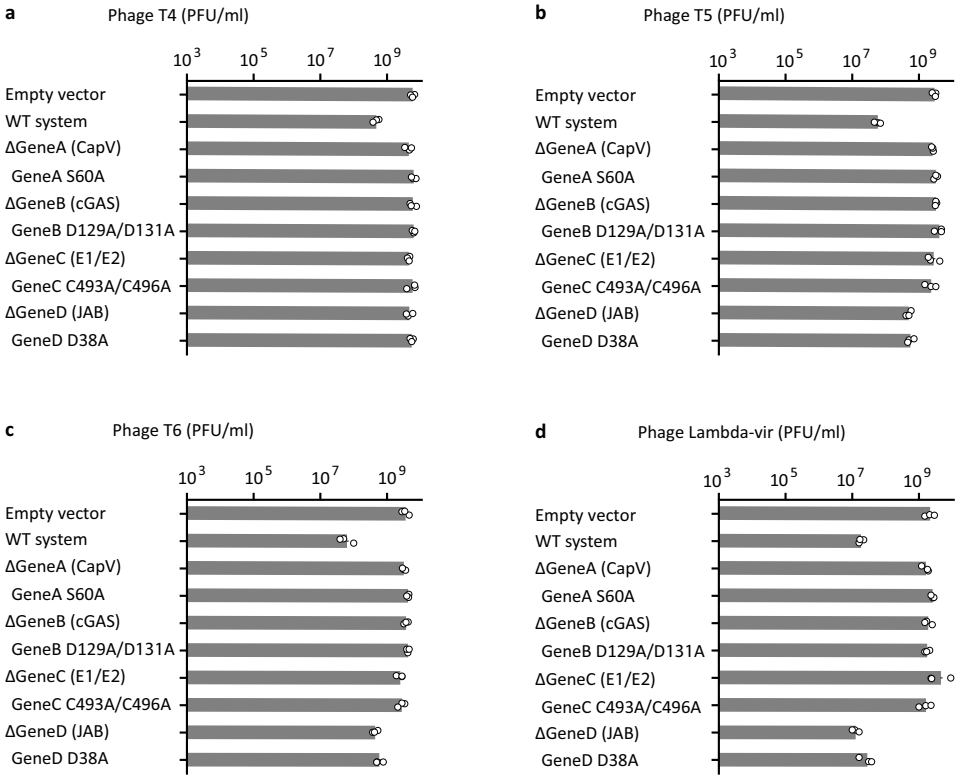

Extended Data Fig. 3 | Efficiency of plating of coliphages on defence systems with whole-gene deletions or point mutations. The efficiency of plating of phages infecting strains with the wild-type *E.-coli*-derived four-gene, deletion strains and strains with point mutations. Data represent plaque-forming units per millilitre; bar graphs represent average of three independent replicates, with individual data points overlaid. Empty vector represents a control *E. coli* MG1655 strain that lacks the system and has an empty vector instead. **a**, Infection with the phage T4. **b**, Infection with the phage T5. **c**, Infection with the phage T6. **d**, Infection with the phage λ-vir.

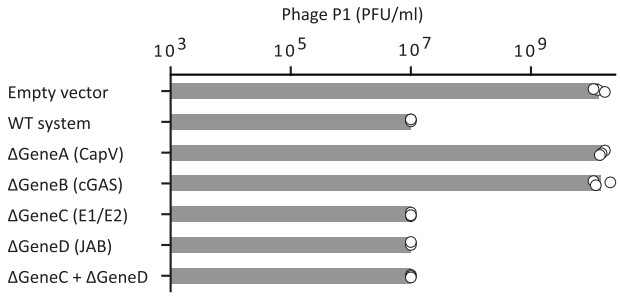

Extended Data Fig. 4 | Efficiency of plating of phage P1 on a double-deletion strain. The efficiency of plating is shown of phage P1 infecting strains with the wild-type *E.-coli*-derived four-gene system, strains with individual genes deleted and a strain with two genes deleted. Data represent plaque-forming units per millilitre; bar graphs represent average of three independent replicates, with individual data points overlaid. Empty vector represents a control *E. coli* MG1655 strain that lacks the system and has an empty vector instead.

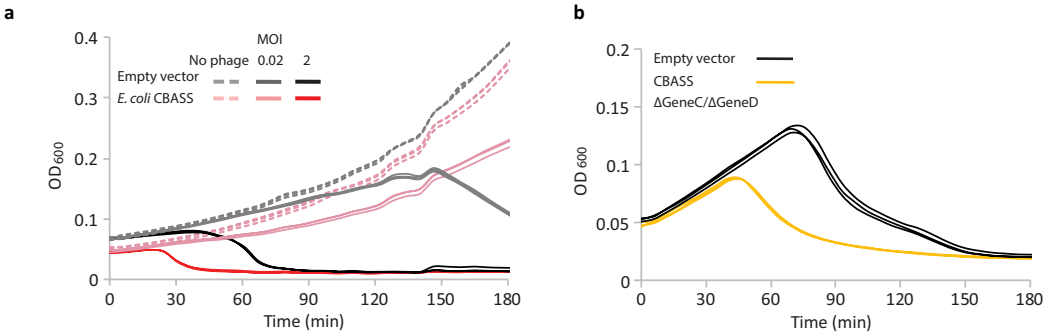

Extended Data Fig. 5 | The bacterial CBASS functions through abortive infection. a, Growth curves in liquid culture for CBASS-containing and CBASS-lacking (empty vector) bacteria infected by phage SECphi18 at 25 °C. Bacteria were infected at time = 0 at an MOI of 0.02 or 2. Three independent replicates for each MOI are shown, and each curve shows an individual replicate. **b**, Growth curves in liquid culture for cells containing a minimal CBASS comprising phospholipase–cGAS (*capV-dncV*) only. Bacteria were infected at time = 0 at an MOI of 2 by phage P1. Three independent replicates for each MOI are shown, and each curve shows an individual replicate.

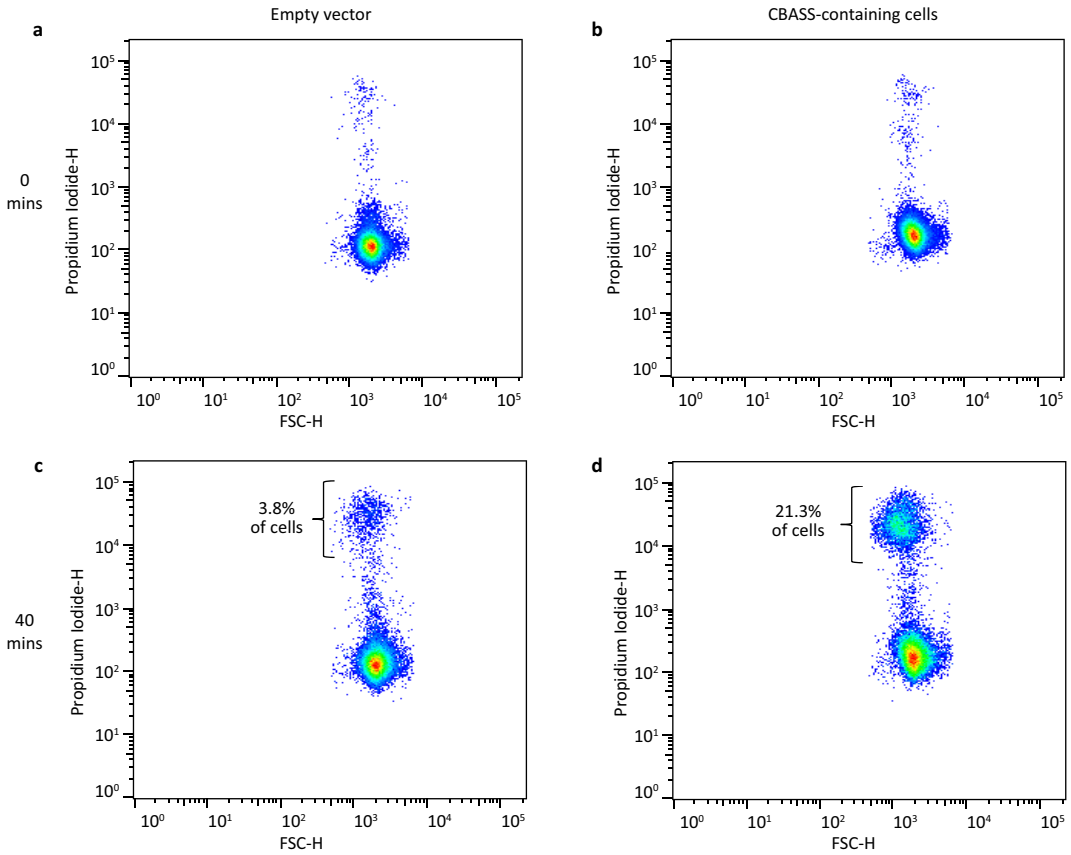

Extended Data Fig. 6 | Cell sorting of infected cells stained with propidium iodide. Cells containing the CBASS derived from *E. coli* TW11681, and control cells containing an empty vector, were stained with propidium iodide, a fluorescent DNA-binding agent that penetrates cells that have impaired membrane integrity. Cells were infected by phage P1 (MOI of 2) and sorted on the basis of propidium-iodide fluorescence intensity (*y* axis); the *x* axis represents forward scatter. **a**, Uninfected cells that lack the CBASS. **b**, Uninfected cells that contain the CBASS. **c**, Cells that lack the CBASS, 40 min after infection. **d**, Cells that contain the CBASS, 40 min after infection. A large population of cells with high propidium-iodide fluorescence intensity is observed. Data from a representative replicate of two independent replicates are shown.

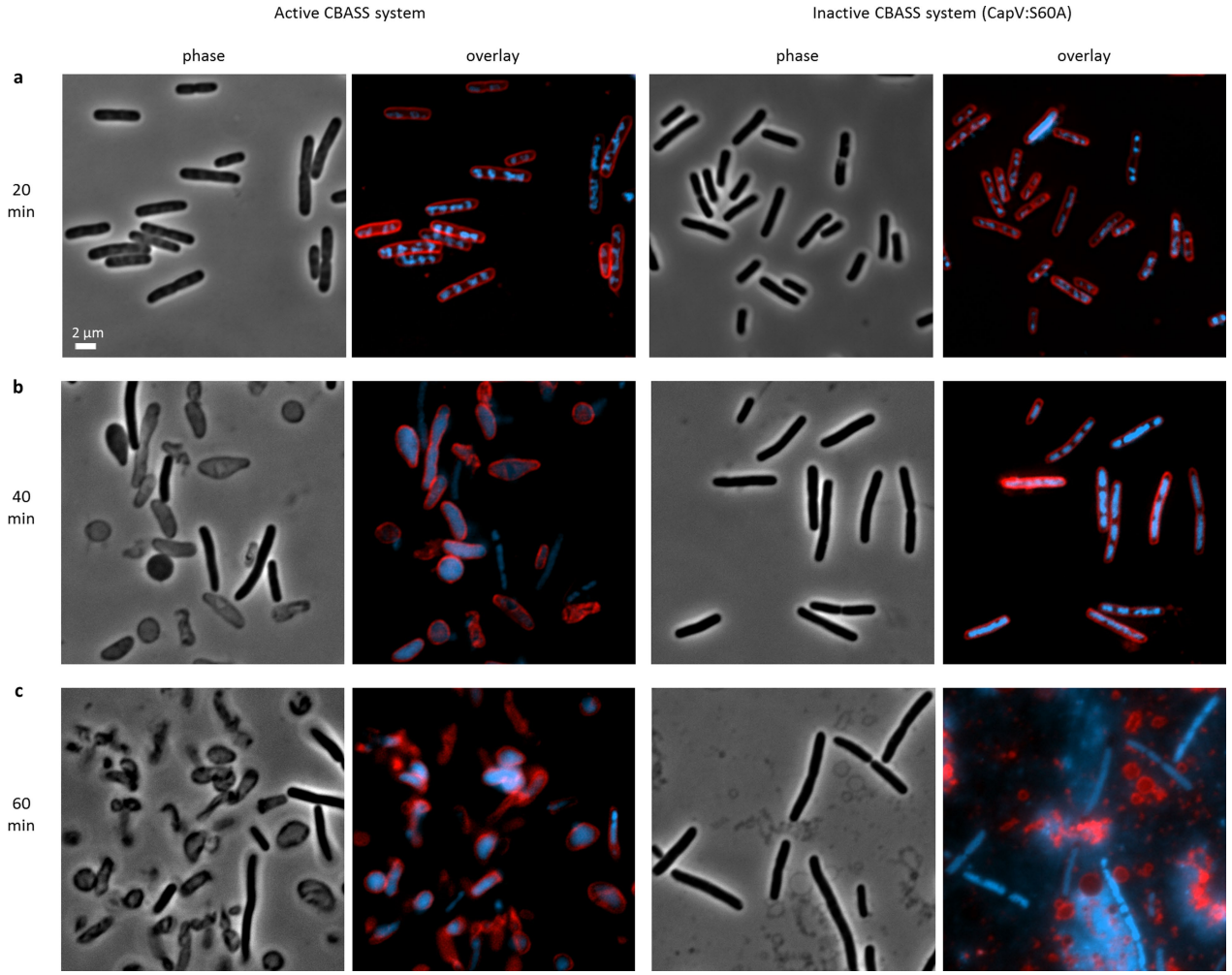

Extended Data Fig. 7 | Microscopy of infected cells. a–c, Phase contrast and overlay images are shown, of membrane stain (red) and DAPI (blue) images captured at 20 min (**a**), 40 min (**b**) and 60 min (**c**) after infection with phage P1 at an MOI of 2. The two columns on the left show *E. coli* MG1655 cells containing the CBASS derived from *E. coli* TW11681. The two columns on the right show *E.coli* MG1655 cells containing the CBASS derived from *E. coli* with a single point mutation that inactivates the CapV phospholipase (CapV(S60A)). Cell shape is deformed after 40 min in cells containing the CBASS, but not in cells in which the CBASS is mutated. After 60 min, phage-mediated cell lysis is observed in cells in which the CBASS is mutated. Representative images from a single replicate out of two independent replicates are shown.

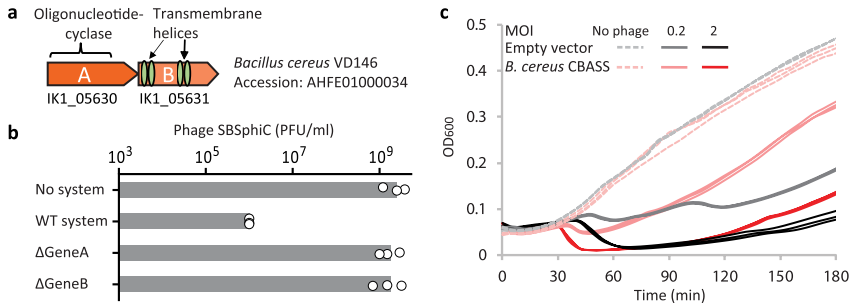

Extended Data Fig. 8 | A two-gene CBASS protects *Bacillus* against phage infection. a, Domain organization of a two-gene operon found in the *B. cereus* VD146 genome. Locus tags of the depicted genes are indicated below each gene. **b**, The two-gene operon from *B. cereus* VD146 was cloned and genomically integrated into *B. subtilis* BEST7003, which naturally lacks this system. The efficiency of plating of phage SBSphiC infecting the CBASS-lacking and CBASS-containing strains, as well as strains in which one of the two genes was deleted, is shown. Bar graph represents average of three independent replicates, with individual data points overlaid. **c**, Growth curves in liquid culture for *B. subtilis* containing the *B. cereus* two-gene CBASS, or CBASS-lacking *B. subtilis* that contains an empty vector instead, infected by phage SBSphiC. Bacteria were infected at time = 0 at an MOI of 0.2 or 2. Three independent replicates for each MOI are shown, and each curve shows an individual replicate.

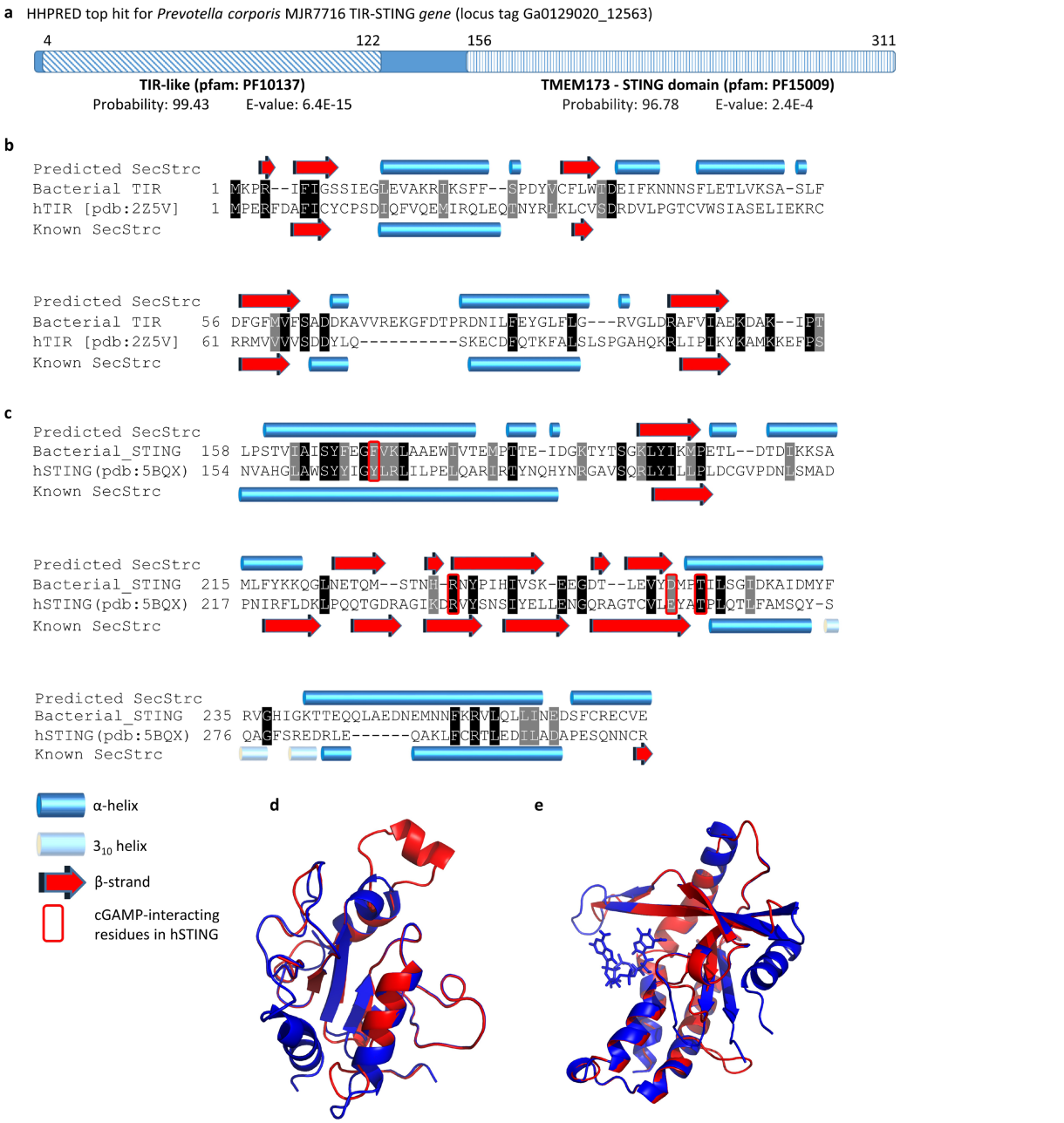

Extended Data Fig. 9 | Domain analysis and homology-based structure prediction of a bacterial TIR–STING protein. a, Schematics of HHpred[29] homology-based search results of the *Prevotella corporis* TIR–STING protein (Supplementary Table 1). **b**, Phyre2[35] secondary structure prediction of the TIR domain in the *P. corporis* TIR–STING protein, compared to the solved crystal structure of the human TIR domain protein MyD88 (PDB accession 2Z5V_A). **c**, Phyre2[35] secondary structure prediction of the STING domain in the *P. corporis* TIR–STING protein, compared to the solved crystal structure of the human STING protein (PDB accession 5BQX_A). Black, identical residues; grey, similar residues. Secondary structure prediction for the bacterial protein appears above the alignment; secondary structure of solved human domain appears below the alignment. **d**, Structural alignment of human TIR domain protein MYD88 and the modelled bacterial TIR domain. **e**, Structural alignment of human STING domain and the modelled bacterial STING domain. In **d**, **e**, blue and red represent the structure of the human protein and the model of the bacterial domain structure, respectively.